

Received November 18, 2020, accepted November 22, 2020, date of publication December 15, 2020, date of current version January 14, 2021.

Digital Object Identifier 10.1109/ACCESS.2020.3045083

# MIMO Dual-Functional Radar-Communication Waveform Design With Peak Average Power Ratio Constraint

YUJIU ZHAO<sup>1</sup>, YIQIN CHEN<sup>1</sup>, MATTHEW RITCHIE<sup>2</sup>, (Senior Member, IEEE), WEIMIN SU<sup>1</sup>, AND HONG GU<sup>1</sup>

<sup>1</sup>Department of Electronic and Optical Engineering, Nanjing University of Science and Technology, Nanjing 210094, China

<sup>2</sup>Department of Electronic and Electrical Engineering, University College London, London WC1E 7JE, U.K.

Corresponding author: Hong Gu (guhong\_zyj\_njust@126.com)

This work was supported in part by the National Natural Science Foundation of China under Grant 61671246 and Grant 61801221, and in part by the Jiangsu Planned Projects for Postdoctoral Research Funds under Grant 2018K043C.

**ABSTRACT** In this paper, novel Dual-Functional Radar-Communication (DFRC) waveforms with peak average power ratio (PAPR) constraint are designed, which are under the multiple-input multiple-output (MIMO) radar-communication system. The DFRC waveforms transmitted by multiple antennas can send communication information to many downlink cellular users and detect radar targets simultaneously. An optimization model is established to minimize the downlink multi-user interference (MUI) under PAPR constraint. The model is non-convex quadratically constrained quadratic programs (QCQP) and can be derived into a convex problem and solved by using the semi-definite relaxation (SDR) technique with rank-one approximation. Numerical simulations demonstrate that our proposed waveforms can achieve a better radar performance in practical scenarios without sacrificing the communication performance.

**INDEX TERMS** Spectral coexistence, dual-functional radar-communication, non-convex optimization, semi-definite relaxation, peak average power ratio constraint.

## I. INTRODUCTION

In recent years, Radio Frequency (RF) spectral congestion has become a serious problem due to the tremendous growth of spectral demands from different wireless applications, and the current inefficient spectral allocations [1]–[6]. Sharing the spectrum among both radar and communication signals can be a promising method of addressing this issue. In general, there are two approaches for achieving shared spectrum access of radar and communication. The first approach is to let the radar systems transmit in the spacial and frequency domains, they are unoccupied by any communication system. To achieve this, a spatial filter can be designed to separate the radar and communication signals [7]–[9]. Nevertheless, such methods will cause potential cross interference and serious degradation in the transmitting process if the radar and communication signals are not perfectly separated.

The second approach is the joint design of dual-functional radar-communication (DFRC) waveforms [10]–[14], which can detect radar targets and transmit communication

information simultaneously. DFRC waveforms can prevent cross interference while taking full advantage of current hardware edge caching capabilities. In [10], [11], communication information are embedded into the radar intrapulse waveforms, while the communication information have the property of low intercept probability. In [12], a sequence of communication bits are embedded into several orthogonal transmitted waveforms. The mainlobe of this DFRC waveform is used for detecting the targets, while the sidelobes are used to transmit information to the communication receivers. In practical scenarios, radar waveforms are often transmitted with nonlinear amplifiers, and the radar waveforms should be designed with constant-modulus (CM) or low peak average power ratio (PAPR). In [14], CM DFRC waveforms are designed by use of a branch-and-bound (BnB) algorithm, which is however computationally inefficient. To further reduce the computational overhead, a Riemannian conjugate gradient (RCG) algorithm has been proposed in [15] for designing CM waveforms. While the CM waveforms are able to fully adapt to the radar's amplifier restrictions, they may incur performance-loss to the output signal noise ratio (SNR).

The associate editor coordinating the review of this manuscript and approving it for publication was Pia Addabbo<sup>1</sup>.

In this paper, we propose novel DFRC waveforms which minimizes the downlink multi-user interference (MUI) under the total transmitted power and PAPR constraints. A trade-off parameter is introduced to control the priority of radar and communication performance. Assuming that the communication channel matrix could be estimated perfectly. While the optimization problem is non-convex and NP (non-deterministic polynomial)-hard in general, it can be efficiently solved by the semidefinite relaxation (SDR) technique. By applying rank-one approximation, the near-optimal solution can be achieved. Numerical results demonstrate that the waveforms proposed in this article can achieve a better radar performance in practical scenarios without sacrificing the communication performance and our algorithm obtains better performance in the DFRC system compared to its CM counterpart.

**II. SYSTEM MODEL**

We consider a multiple-input multiple-output (MIMO) DFRC system which is shown in Fig. 1, the RadCom Base Station is equipped with  $N$  antennas which are located in a uniform linear array (ULA). This system has the objective of detecting radar targets, and communicate with  $K$  single-antenna users simultaneously. The communication and radar signal models will be introduced, respectively.

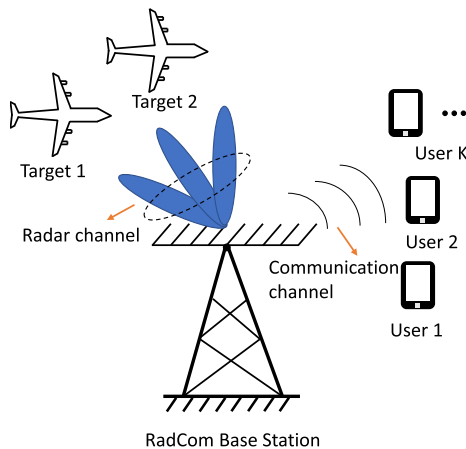


**FIGURE 1. MIMO dual-functional Radar-Communication system.**

**A. COMMUNICATION MODEL**

The received signal matrix at legitimate downlink users can be defined as:

$$\mathbf{Y} = \mathbf{H}\mathbf{X} + \mathbf{Z}, \tag{1}$$

where  $\mathbf{H} = [\mathbf{h}_1, \mathbf{h}_2, \dots, \mathbf{h}_K]^T \in \mathbb{C}^{K \times N}$  represents the channel matrix, which is assumed to be flat Rayleigh fading and estimated perfectly,  $\mathbf{X} = [\mathbf{x}_1, \mathbf{x}_2, \dots, \mathbf{x}_L] \in \mathbb{C}^{N \times L}$  denotes the transmitted signal matrix, with  $L$  being the length of the radar pulse or communication frame, and  $\mathbf{Z} = [\mathbf{z}_1, \mathbf{z}_2, \dots, \mathbf{z}_L] \in \mathbb{C}^{K \times L}$  denotes the noise matrix, with  $\mathbf{z}_l \sim \mathcal{CN}(0, N_0 \mathbf{I}_N), \forall l \in (1, 2, \dots, L)$ , where  $\mathcal{CN}()$  denotes Gaussian distribution. If the channel matrix  $\mathbf{H}$  is estimated imperfectly, a min-max optimization could be used

as a variable approach [9], [16] and it will be a future avenue of research. With a known constellation symbol matrix  $\mathbf{S} \in \mathbb{C}^{K \times L}$ , it is desired by the legitimate downlink users. Therefore, the received signals can be rewritten as

$$\mathbf{Y} = \mathbf{S} + \underbrace{\mathbf{H}\mathbf{X} - \mathbf{S}}_{\text{MUI}} + \mathbf{Z}, \tag{2}$$

The entry of  $\mathbf{S} \in \mathbb{C}^{K \times L}$  for each downlink user can be assumed to be taken from the same alphabet, such as a quadrature phase shift keying (QPSK) constellation. The second term in (2) is defined as the multi-user interference (MUI) signals, and the total MUI energy can be expressed as

$$P_{\text{MUI}} = \|\mathbf{H}\mathbf{X} - \mathbf{S}\|_F^2, \tag{3}$$

Since the achievable sum-rate of the legitimate downlink users is affected by the MUI energy directly [17], the Signal-to-Interference-plus-Noise-Ratio (SINR) in each pulse for the  $i$ -th user can be expressed as

$$\eta_i = \frac{\mathbb{E}(|s_{i,j}|^2)}{\underbrace{\mathbb{E}(|\mathbf{h}_i^T \mathbf{x}_j - s_{i,j}|^2)}_{\text{MUI energy}} + N_0}, \tag{4}$$

where  $s_{i,j}$  denotes the  $(i, j)$  th entry of  $\mathbf{S}$ , and  $\mathbb{E}$  represents the total average in relation to the pulse width. Therefore, the achievable sum-rate of the users is defined as

$$\Gamma = \sum_{i=1}^K \log_2(1 + \eta_i), \tag{5}$$

It can be observed that the power of our signal  $\mathbb{E}(|s_{i,j}|^2)$  is a constant parameter when the energy of a known constellation is fixed. Thus, maximizing the sum-rate turns into minimizing the MUI energy.

**B. MIMO RADAR MODEL**

It is well known that MIMO radar has many advantages such as improving the spatial resolution and enhancing the ability of anti-jamming due to the high Degrees of Freedom (DOFs) [18], [19]. In addition to these points, the overall waveform diversity of the system has also been improved which can be advantageous in a congested or contested environment. The general approach of MIMO radar waveform design is focused on designing the beampattern, which is equivalent to the covariance matrix of the transmitted signals, and it can be solved by the convex optimization [20]. Here our radar model only consists of the thermal noise, but in the practical scenarios clutter and jamming could also affect the radar performance. More complicated radar models can be used, and some robust estimates, based on geometric considerations as well as statistical properties of covariance matrix can be used to improve the performance of the classic sample covariance [21]–[23]. In our MIMO radar systems, the waveforms should be designed with the low auto-correlation and cross-correlation sidelobes under the CM or lower PAPR

constraint [24]–[26]. Here, we focus on designing a directional beampattern, our desired spatial covariance matrix of the DFRC transmitted signals is expressed as

$$\mathbf{R}_X = \frac{1}{L} \mathbf{X} \mathbf{X}^H = \frac{P_t}{N} \mathbf{I}_N, \quad (6)$$

where  $\mathbf{I}_N$  represents the  $N$  dimensional identity matrix. Thus, the orthogonal linear frequency modulation (LFM) waveforms  $\mathbf{X}_0$  are regarded as our reference waveforms. The  $(n, l)$ -th sampling point of  $X_0(n, l)$  can be expressed as:

$$X_0(n, l) = \frac{\exp\{j2\pi n(l-1)/L\} \exp\{j\pi(l-1)^2/L\}}{\sqrt{NP_t}} \quad (7)$$

where  $n = 1, \dots, N, l = 1, \dots, L$ , and  $P_t$  is the total transmit power. Our novel DFRC waveforms are based on the radar and communication systems defined above.

### III. TRADE-OFF BETWEEN RADAR AND COMMUNICATION PERFORMANCE WITH PAPR CONSTRAINT

**A. CONVENTIONAL TRADE-OFF DFRC WAVEFORM DESIGN**  
We first provide the optimization problem of conventional trade-off DFRC waveform design under the total transmitted power constraint

$$\begin{aligned} \min_{\mathbf{X}} \quad & \rho \|\mathbf{H}\mathbf{X} - \mathbf{S}\|_F^2 + (1 - \rho) \|\mathbf{X} - \mathbf{X}_0\|_F^2, \\ \text{s.t.} \quad & \frac{1}{L} \|\mathbf{X}\|_F^2 = P_t, \end{aligned} \quad (8)$$

where  $\rho \in [0, 1]$  is the weighting coefficient that controls the balance of radar and communication performance in DFRC waveforms. Assuming that  $\mathbf{A} = [\sqrt{\rho}\mathbf{H}^T, \sqrt{1-\rho}\mathbf{I}_N]^T \in \mathbb{C}^{(K+N) \times N}$ ,  $\mathbf{B} = [\sqrt{\rho}\mathbf{S}^T, \sqrt{1-\rho}\mathbf{X}_0^T]^T \in \mathbb{C}^{(K+N) \times L}$ , (8) can be rewritten as:

$$\begin{aligned} \min_{\mathbf{X}} \quad & \|\mathbf{A}\mathbf{X} - \mathbf{B}\|_F^2, \\ \text{s.t.} \quad & \|\mathbf{X}\|_F^2 = LP_t, \end{aligned} \quad (9)$$

It is a non-convex quadratically constrained quadratic program (QCQP) which can be converted into a Semidefinite Programming (SDP). This optimization problem can be solved by the method of Semidefinite Relaxation (SDR), and further details can be found in [14].

### B. TRADE-OFF DFRC WAVEFORM DESIGN WITH PAPR CONSTRAINT

According to the analysis above, we combine the conventional trade-off DFRC waveform design with the PAPR constraint. PAPR is a significant parameter in the aspect of transmitting radar waveforms, and large PAPR can distort radar waveforms. The optimization problem can be expressed as:

$$\begin{aligned} \min_{\mathbf{X}} \quad & \|\mathbf{A}\mathbf{X} - \mathbf{B}\|_F^2, \\ \text{s.t.} \quad & \|\mathbf{X}\|_F^2 = LP_t, \\ & \text{PAPR}(\mathbf{X}) \leq r; \end{aligned} \quad (10)$$

where  $r \in [1, NL]$ . In the case where  $r = 1$ , it transforms into the CM constraint. The PAPR constraint can be given as follow [26], [27]

$$\text{PAPR}(\mathbf{x}) = \frac{\max_m |x(m)|^2}{\frac{\|\mathbf{x}\|^2}{NL}} \leq r, \quad (11)$$

where  $\mathbf{x} = \text{vec}(\mathbf{X}) \in \mathbb{C}^{NL \times 1}$ ,  $m = 1, \dots, NL$ . It can be observed that the total transmitted power and PAPR constraints have transformed into a quadratic equality constraint and a series of quadratic inequality constraints, respectively:

$$\begin{aligned} \mathbf{x}^H \mathbf{x} &= LP_t, \\ \mathbf{x}^H \mathbf{E}_m \mathbf{x} &\leq \frac{P_t r}{N}. \end{aligned} \quad (12)$$

where

$$\mathbf{E}_m(i, j) = \begin{cases} 1 & i = m \text{ and } j = m \\ 0 & \text{otherwise.} \end{cases} \quad (13)$$

where  $\mathbf{E}_m \in \mathbb{R}^{NL \times NL}$ . In order to combine the vectorized PAPR constraint with the objective function together, the objective function of (10) must be vectorized. The  $\mathbf{A}$  can be written into one diagonal matrix:

$$\tilde{\mathbf{A}} = \begin{bmatrix} \mathbf{A} & & & \\ & \mathbf{A} & & \\ & & \ddots & \\ & & & \mathbf{A} \\ & & & & \mathbf{A} \end{bmatrix} \in \mathbb{C}^{(K+N)L \times NL} \quad (14)$$

and  $\mathbf{b} = \text{vec}(\mathbf{B}) \in \mathbb{C}^{(K+N)L \times 1}$ . Thus, (10) can be rewritten as:

$$\begin{aligned} \min_{\mathbf{x}} \quad & \|\tilde{\mathbf{A}}\mathbf{x} - \mathbf{b}\|^2, \\ \text{s.t.} \quad & \mathbf{x}^H \mathbf{x} = LP_t, \\ & \mathbf{x}^H \mathbf{E}_m \mathbf{x} \leq \frac{P_t r}{N}. \end{aligned} \quad (15)$$

where (15) is a non-convex QCQP with a non-convex quadratic equality constraint and a series of quadratic inequality constraints.

### IV. SOLUTION TO THE OPTIMIZATION MODEL

The SDR techniques have been shown to be an effective method to solve the problem of waveform design with a non-convex QCQP. According to the analysis in [28], we apply the matlab CVX tools [29] to solve this problem after a series of derivations. Thus, we have the following transform:

$$\mathbf{G} = \begin{bmatrix} \Re(\tilde{\mathbf{A}}) & -\Im(\tilde{\mathbf{A}}) \\ \Im(\tilde{\mathbf{A}}) & \Re(\tilde{\mathbf{A}}) \end{bmatrix} \in \mathbb{R}^{2(K+N)L \times 2NL}, \quad (16)$$

$$\mathbf{s} = [\Re(\mathbf{x}) \quad \Im(\mathbf{x})]^T \in \mathbb{R}^{2NL \times 1}, \quad (17)$$

$$\mathbf{y} = [\Re(\mathbf{b}) \quad \Im(\mathbf{b})]^T \in \mathbb{R}^{2(K+N)L \times 1}. \quad (18)$$

where  $\Re(\mathbb{C})$  and  $\Im(\mathbb{C})$  denote the real value and the imaginary value, respectively. The objective function of (15) can be rewritten as:

$$\min_{\mathbf{s}} \|\mathbf{G}\mathbf{s} - \mathbf{y}\|^2, \quad (19)$$

Here, (19) is an inhomogeneous QCQP. In order to homogenize (19), we introduce one new parameter  $v$  and assume that  $v^2 = 1$ . Then, (19) is equivalent to the following expression:

$$\min_{\mathbf{s}, v} \|\mathbf{v}\mathbf{y} - \mathbf{G}\mathbf{s}\|^2, \quad \text{s.t. } v^2 = 1. \quad (20)$$

Thus, (20) can be expressed as a homogeneous QCQP:

$$\min_{\mathbf{s}, v} \begin{bmatrix} \mathbf{G}^T \mathbf{G} & -\mathbf{G}^T \mathbf{y} \\ -\mathbf{y}^T \mathbf{G} & \|\mathbf{y}\|^2 \end{bmatrix} \begin{bmatrix} \mathbf{s} \\ v \end{bmatrix}, \quad \text{s.t. } v^2 = 1. \quad (21)$$

Assuming that  $\tilde{\mathbf{s}} = [\mathbf{s}^T \ v]^T \in \mathbb{R}^{(2NL+1) \times 1}$  and

$$\mathbf{D} = \begin{bmatrix} \mathbf{G}^T \mathbf{G} & -\mathbf{G}^T \mathbf{y} \\ -\mathbf{y}^T \mathbf{G} & \|\mathbf{y}\|^2 \end{bmatrix} \quad (22)$$

Then, (19) turns into the following expression:

$$\min_{\tilde{\mathbf{s}}, v} \tilde{\mathbf{s}}^T \mathbf{D} \tilde{\mathbf{s}}, \quad \text{s.t. } v^2 = 1. \quad (23)$$

For the quadratic constraint in (15), based on the constraint condition in (23), and  $\tilde{\mathbf{s}}$  is used to replace the parameter  $\mathbf{x}$ . Thus, we have the following expression:

$$\begin{aligned} \tilde{\mathbf{s}}^T \tilde{\mathbf{s}} &= LP_t + 1, \\ \tilde{\mathbf{s}}^T \tilde{\mathbf{E}}_w \tilde{\mathbf{s}} &\leq \frac{P_t r}{N} \end{aligned} \quad (24)$$

where

$$\tilde{\mathbf{E}}_w(i, j) = \begin{cases} 1 & i = w \text{ and } j = w \\ 1 & i = NL + w \text{ and } j = NL + w \\ 0 & \text{otherwise.} \end{cases} \quad (25)$$

where  $\tilde{\mathbf{E}}_w \in \mathbb{R}^{(2NL+1) \times (2NL+1)}$  and  $w \in [1, \dots, 2NL + 1]$ . Combining (23) and (24) together, the optimization model of DFRC waveform design with the total transmitted power and PAPR constraints becomes:

$$\begin{aligned} \min_{\tilde{\mathbf{s}}, v} \quad & \tilde{\mathbf{s}}^T \mathbf{D} \tilde{\mathbf{s}}, \\ \text{s.t.} \quad & v^2 = 1, \\ & \tilde{\mathbf{s}}^T \tilde{\mathbf{s}} = LP_t + 1, \\ & \tilde{\mathbf{s}}^T \tilde{\mathbf{E}}_w \tilde{\mathbf{s}} \leq \frac{P_t r}{N} \end{aligned} \quad (26)$$

To further improve the objective function, the following assumptions can be made  $\tilde{\mathbf{S}} = \tilde{\mathbf{s}}^T \tilde{\mathbf{s}}$ , and  $\text{tr}(\tilde{\mathbf{S}}) = \text{tr}(\tilde{\mathbf{s}}^T \tilde{\mathbf{s}})$ . (26) can be rewritten as:

$$\begin{aligned} \min_{\tilde{\mathbf{s}}, v} \quad & \text{tr}(\mathbf{D}\tilde{\mathbf{S}}), \\ \text{s.t.} \quad & \tilde{\mathbf{S}}(2NL + 1, 2NL + 1) = 1, \\ & \text{tr}(\tilde{\mathbf{S}}) = LP_t + 1, \\ & \text{tr}(\tilde{\mathbf{E}}_w \tilde{\mathbf{S}}) \leq \frac{P_t r}{N} \quad w = 1, \dots, 2NL, \\ & \text{rank}(\tilde{\mathbf{S}}) = 1. \end{aligned} \quad (27)$$

It can be observed that the only non-convex constraint is  $\text{rank}(\tilde{\mathbf{S}}) = 1$ . By using the rank-one approximation, we get

$$\begin{aligned} \min_{\tilde{\mathbf{s}}, v} \quad & \text{tr}(\mathbf{D}\tilde{\mathbf{S}}), \\ \text{s.t.} \quad & \tilde{\mathbf{S}}(2NL + 1, 2NL + 1) = 1, \\ & \text{tr}(\tilde{\mathbf{S}}) = LP_t + 1, \\ & \text{tr}(\tilde{\mathbf{E}}_w \tilde{\mathbf{S}}) \leq \frac{P_t r}{N} \quad w = 1, \dots, 2NL. \end{aligned} \quad (28)$$

It is apparent that the optimal solution can be solved using the SDR technique with rank-one approximation. Then, we can get the optimal solution  $\tilde{\mathbf{S}}_{\text{opt}}$ , and inverse vectorization is applied to obtain  $\tilde{\mathbf{s}}_{\text{opt}}$ , where  $\tilde{\mathbf{s}}_{\text{opt}} = [\mathbf{s}_{\text{opt}} \ v]^T$ . The optimal waveforms can be expressed as  $x_{\text{opt}_p} = s_{\text{opt}_p} + \sqrt{-1}s_{\text{opt}_{p+NL}}$ , where  $p \in [1, NL]$ . The proposed DFRC waveform design is a SDR problem and can be solved by matlab convex optimization toolboxes with an interior-point algorithm, which needs a total  $\mathcal{O}((2NL + 1)^{3.5} \log(1/\epsilon))$  complex floating-point-operations(flops), where one complex flop is defined as one complex addition or multiplication and  $\epsilon > 0$  is a solution accuracy.

## V. SIMULATION RESULTS

In this section, numerical simulations are provided to illustrate that our novel DFRC waveforms have improved radar performance without sacrificing the communication performance than the conventional DFRC waveforms proposed in [14]. ‘Chirp-Tradeoff-Total’ and ‘Chirp-Tradeoff-Total-PAPR’ denote the conventional DFRC waveforms and the DFRC waveforms with the total transmitted power and PAPR constraints, respectively. When  $r = 1$ , the PAPR constraint transforms into the CM constraint, and ‘Chirp-Tradeoff-Total-CM’ denotes the DFRC waveforms with the total transmitted power and CM constraints. Without loss of generality, assuming that the total transmitted power  $P_t = 1$ , and  $\text{SNR} = P_t/N$ . There are  $N = 8$  antennas in the DFRC system, and the system transmits information to  $K = 4$  single-antenna receivers. The length of DFRC waveform pulse is set to be  $L = 20$ . Each entry of  $\mathbf{H}$  subjects to the standard complex Gaussian distribution, and the constellation in  $\mathbf{S} \in \{1 + j, 1 - j, -1 + j, -1 - j\}$  is selected to be the QPSK alphabet, and they correspond to the communication signal bits  $\{00, 01, 10, 11\}$ .

The communication performance achieved by different approaches are shown in Fig. 2 and Fig. 3. ‘Zero-MUI’ represents the ideal situation where the MUI energy is zero. The trade-off parameter  $\rho$  is set to be 0.5. In Fig. 2, when  $\text{SNR} = 10$  dB, with the increasing of  $r$ , the average achievable sum-rate (AASR) of our novel DFRC waveforms with the total transmitted power and PAPR constraints approaches to the AASR of conventional DFRC waveforms. When  $r = 1.5$ , they almost cross together, and the data can be observed in Table 1. Thus, we assume that  $r = 1.5$  is the upper bound to limit the communication performance. Here, we need to highlight when  $r = 1$ ,  $\text{PAPR} = 0$  dB, and our novel DFRC waveforms are under the CM constraint.

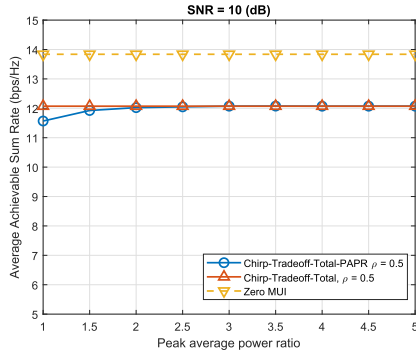


**FIGURE 2.** Average achievable sum-rate and PAPR for different waveforms. ‘Chirp-Tradeoff-Total’ and ‘Chirp-Tradeoff-Total-PAPR’ denote the conventional DFRC waveforms and the DFRC waveforms with the total transmitted power and PAPR constraints, respectively. ‘Zero-MUI’ represents the ideal situation where the MUI energy is zero.  $\rho$  is the trade-off parameter.

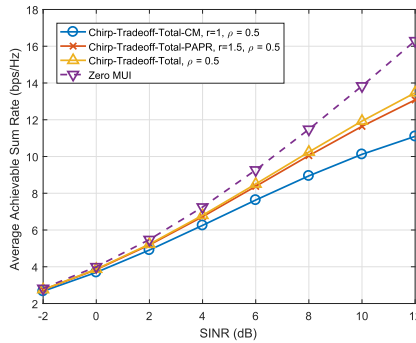


**FIGURE 3.** Average achievable sum-rate comparison for different waveforms in the same SINR. ‘Chirp-Tradeoff-Total-CM’ denotes the DFRC waveforms with the total transmitted power and CM constraints; ‘Chirp-Tradeoff-Total-PAPR’ denotes the DFRC waveforms with the total transmitted power and PAPR constraints; ‘Chirp-Tradeoff-Total’ denotes the conventional DFRC waveforms.  $r$  is the PAPR constraint parameter.  $\rho$  is the trade-off parameter.

**TABLE 1.** The value of average achievable sum-rate for different waveforms in the same PAPR,  $\rho = 0.5$ .

		PAPR				
		1	1.5	2	2.5	5
AASR (bps/Hz)	Waveforms					
	Zero-MUI	13.84	13.84	13.84	13.84	13.84
	Chirp-Tradeoff-Total	12.69	12.69	12.69	12.69	12.69
	Chirp-Tradeoff-Total-PAPR	11.93	12.38	12.61	12.66	12.69

In Fig. 3, our novel DFRC waveforms with different PAPR constraints are shown. Our novel DFRC waveforms which under the total transmitted power and CM constraints obtain the worst AASR comparing with the other situations. The data can be observed in Table 2. With the increase of  $r$ , the AASR of our novel DFRC waveforms approaches to the AASR of conventional DFRC waveforms.

The radar performance achieved by different approaches and parameters are shown in Fig. 4, Fig. 5 and Fig. 6. The Orthogonal-Chirp-Waveforms in (6) are used as the reference waveforms, and the detection probability  $P_D$  is applied to determine the detection performance as a metric [8, eq.(69)]. Assuming that the target is point-like and in the far-field,

**TABLE 2.** The value of average achievable sum-rate for different waveforms in the same SINR,  $\rho = 0.5$ .

		SINR(dB)				
		-2	2	4	8	12
AASR (bps/Hz)	Waveforms					
	Zero-MUI	2.8	5.5	7.3	11.5	16.3
	Chirp-Tradeoff-Total	2.8	5.3	6.9	10.4	13.8
	Chirp-Tradeoff-Total-PAPR, $r = 1.5$	2.8	5.3	6.9	10.4	13.7
	Chirp-Tradeoff-Total-CM, $r = 1$	2.8	5.1	6.5	9.5	12.0

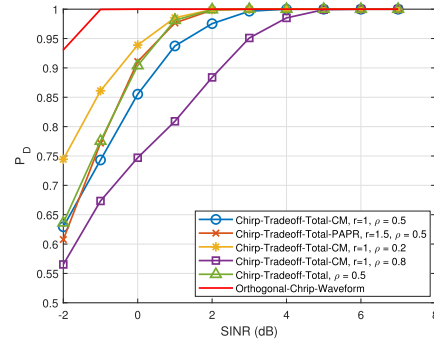


**FIGURE 4.** Radar detection probability and SINR for different approaches and parameters,  $N = 8$ ,  $L = 20$ ,  $P_{FA} = 10^{-7}$ . ‘Chirp-Tradeoff-Total-CM’ denotes the DFRC waveforms with the total transmitted power and CM constraints; ‘Chirp-Tradeoff-Total-PAPR’ denotes the DFRC waveforms with the total transmitted power and PAPR constraints; ‘Chirp-Tradeoff-Total’ denotes the conventional DFRC waveforms; ‘Orthogonal-Chirp-Waveform’ denotes the reference waveforms.  $r$  is the PAPR constraint parameter.  $\rho$  is the trade-off parameter.

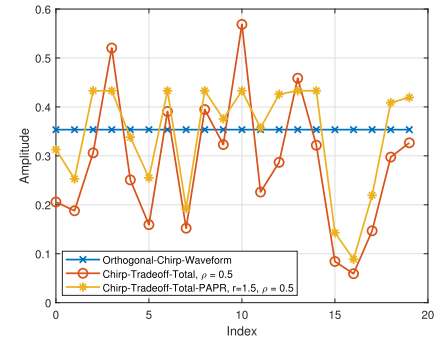


**FIGURE 5.** The waveforms in time domain with different approaches. ‘Orthogonal-Chirp-Waveform’ denotes the reference waveforms; ‘Chirp-Tradeoff-Total’ denotes the conventional DFRC waveforms; ‘Chirp-Tradeoff-Total-PAPR’ denotes the DFRC waveforms with the total transmitted power and PAPR constraints.  $r$  is the PAPR constraint parameter.  $\rho$  is the trade-off parameter.

**TABLE 3.** The value of  $P_D$  for different waveforms in the same SINR.

		SINR(dB)			
		-2	0	2	4
$P_D$	Waveforms				
	Orthogonal-Chirp-Waveform	0.93	1.00	1.00	1.00
	Chirp-Tradeoff-Total, $\rho = 0.5$	0.63	0.90	1.00	1.00
	Chirp-Tradeoff-Total-CM, $r = 1, \rho = 0.8$	0.57	0.75	0.88	0.99
	Chirp-Tradeoff-Total-CM, $r = 1, \rho = 0.2$	0.74	0.93	1.00	1.00
	Chirp-Tradeoff-Total-PAPR, $r = 1.5, \rho = 0.5$	0.61	1.00	1.00	1.00
	Chirp-Tradeoff-Total-CM, $r = 1, \rho = 0.5$	0.63	0.86	0.98	1.00

and the angle of target is  $45^\circ$ . The false-alarm probability of radar is set to be  $P_{FA} = 10^{-7}$ . With the increase of  $r$  or the decrease of  $\rho$ , our novel DFRC waveforms approach to the reference waveforms. The data can be observed in Table 3.



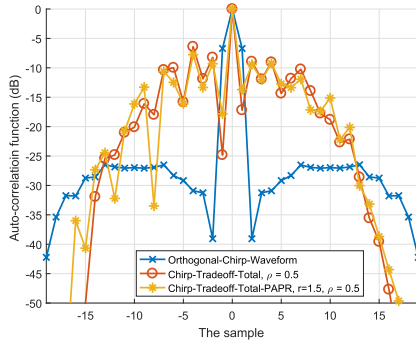


**FIGURE 6.** The auto-correlation function of the waveforms with different approaches. ‘Orthogonal-Chirp-Waveform’ denotes the reference waveforms; ‘Chirp-Tradeoff-Total’ denotes the conventional DFRC waveforms; ‘Chirp-Tradeoff-Total-PAPR’ denotes the DFRC waveforms with the total transmitted power and PAPR constraints.  $r$  is the PAPR constraint parameter.  $\rho$  is the trade-off parameter.

**TABLE 4.** The value of ACLSs and PAPR for different waveforms.

Waveforms	Parameter	ACSLs(dB)	$r$
Orthogonal-Chirp-Waveform		-26.52	1.0
Chirp-Tradeoff-Total, $\rho = 0.5$		-6.41	4.0
Chirp-Tradeoff-Total-PAPR, $r = 1.5,\rho = 0.5$		-7.75	1.5

When  $r = 1.5$  and  $\rho = 0.5$ , the detection probability value of our novel DFRC waveforms and the conventional DFRC waveforms are overlapped together. It means that they have the same performance of radar detection ability in the simulation. In Fig. 5, the waveforms designed with different approaches are shown in time domain. According to the function in (6), the modulus of Orthogonal-Chirp-Waveforms is constant. Thus, the blue line which stands for the Orthogonal-Chirp-Waveforms is a straight line and regarded as the reference. The orange line denotes the Chirp-Tradeoff-Total waveform and the yellow line denotes the Chirp-Tradeoff-Total-PAPR waveform. The data is shown in Table 4. It can be observed that the conventional DFRC waveform has higher peak altitude than our novel DFRC waveform. As assumed above, our novel DFRC waveforms are designed under the PAPR constraint with  $r = 1.5$ , while the PAPR of conventional DFRC waveform is  $r = 4$  via calculations. The auto-correlation sidelobes (ACSLs) in range direction are shown in Fig. 6, all the signals are processed by hamming window. It can be observed that the ACSL of Orthogonal-Chirp-Waveforms is  $-26.52\text{dB}$ , the ACSL of Chirp-Tradeoff-Total waveforms is  $-6.41\text{dB}$ , and the ACSL of Chirp-Tradeoff-Total-PAPR is  $-7.75\text{dB}$ . It means that our proposed DRFC waveforms have the lower sidelobes than the conventional DRFC waveforms. In addition, in practical systems, the conventional DRFC waveforms will suffer from more severe degradation due to a large distortion accrued in the signal transmitting process. Thus, our novel DFRC waveforms achieve better radar performances with lower PAPR.

## VI. CONCLUSION

In this paper, the novel DFRC waveforms with the total transmitted power and PAPR constraints are designed. By minimizing the MUI energy and controlling the trade-off parameter to allocate the priority of performance between radar and communication system. The optimization model is a non-convex problem with one quadratic equality constraint and a series of quadratic inequality constraints. This problem has been solved using the SDR technique. Numerical simulations demonstrate that our novel DFRC waveforms achieve better performance in radar system without sacrificing the communication performance. In the future, we will do more researches on the DFRC waveform design when the imperfect estimations of the channel matrix are considered.

## REFERENCES

- [1] FCC. (2010). *Connecting America: The National Broadband Plan*. [Online]. Available: <https://www.fcc.gov/general/national-broadband-plan>
- [2] NSF. (2019). *Spectrum Efficiency, Energy Efficiency, and Security (SpecEES): Enabling Spectrum for All*. [Online]. Available: <https://www.nsf.gov/pubs/2019/nsf19529/nsf19529.htm>
- [3] H. Griffiths, S. Blunt, L. Cohen, and L. Savy, “Challenge problems in spectrum engineering and waveform diversity,” in *Proc. IEEE Radar Conf.*, Ottawa, ON, USA, Apr. 2013, pp. 1–5.
- [4] H. Griffiths, L. Cohen, S. Watts, E. Mokole, C. Baker, M. Wicks, and S. Blunt, “Radar spectrum engineering and management: Technical and regulatory issues,” *Proc. IEEE*, vol. 103, no. 1, pp. 85–102, Jan. 2015.
- [5] M. Wicks, “Spectrum crowding and cognitive radar,” in *Proc. 2nd Int. Workshop Cognit. Inf. Process.*, Jun. 2010, pp. 452–457.
- [6] A. Aubry, V. Carotenuto, A. De Maio, A. Farina, and L. Pallotta, “Optimization theory-based radar waveform design for spectrally dense environments,” *IEEE Aerosp. Electron. Syst. Mag.*, vol. 31, no. 12, pp. 14–25, Dec. 2016.
- [7] Z. Geng, H. Deng, and B. Himed, “Adaptive radar beamforming for interference mitigation in radar-wireless spectrum sharing,” *IEEE Signal Process. Lett.*, vol. 22, no. 4, pp. 484–488, Apr. 2015.
- [8] A. Khawar, A. Abdelhadi, and C. Clancy, “Target detection performance of spectrum sharing MIMO radars,” *IEEE Sensors J.*, vol. 15, no. 9, pp. 4928–4940, Sep. 2015.
- [9] F. Liu, C. Masouros, A. Li, and T. Ratnarajah, “Robust MIMO beamforming for cellular and radar coexistence,” *IEEE Wireless Commun. Lett.*, vol. 6, no. 3, pp. 374–377, Jun. 2017.
- [10] S. D. Blunt, P. Yatham, and J. Stiles, “Intrapulse radar-embedded communications,” *IEEE Trans. Aerosp. Electron. Syst.*, vol. 46, no. 3, pp. 1185–1200, Jul. 2010.
- [11] D. Ciuonzo, A. De Maio, G. Foglia, and M. Piezzo, “Intrapulse radar-embedded communications via multiobjective optimization,” *IEEE Trans. Aerosp. Electron. Syst.*, vol. 51, no. 4, pp. 2960–2974, Oct. 2015.
- [12] A. Hassanien, M. G. Amin, Y. D. Zhang, and F. Ahmad, “Dual-function radar-communications: Information embedding using sidelobe control and waveform diversity,” *IEEE Trans. Signal Process.*, vol. 64, no. 8, pp. 2168–2181, Apr. 2016.
- [13] A. R. Chiriyath, B. Paul, G. M. Jacyna, and D. W. Bliss, “Inner bounds on performance of radar and communications co-existence,” *IEEE Trans. Signal Process.*, vol. 64, no. 2, pp. 464–474, Jan. 2016.
- [14] F. Liu, L. Zhou, C. Masouros, A. Li, W. Luo, and A. Petropulu, “Toward dual-functional radar-communication systems: Optimal waveform design,” *IEEE Trans. Signal Process.*, vol. 66, no. 16, pp. 4264–4279, Aug. 2018.
- [15] F. Liu, C. Masouros, and H. Griffiths, “Dual-functional radar-communication waveform design under constant-modulus and orthogonality constraints,” 2019, *arXiv:1904.05917*. [Online]. Available: <http://arxiv.org/abs/1904.05917>
- [16] X. Cheng, A. Aubry, D. Ciuonzo, A. De Maio, and X. Wang, “Robust waveform and filter bank design of polarimetric radar,” *IEEE Trans. Aerosp. Electron. Syst.*, vol. 53, no. 1, pp. 370–384, Feb. 2017.

[17] S. K. Mohammed and E. G. Larsson, "Per-antenna constant envelope precoding for large multi-user MIMO systems," *IEEE Trans. Commun.*, vol. 61, no. 3, pp. 1059–1071, Mar. 2013.

[18] J. Li and P. Stoica, *MIMO Radar Signal Processing*. Hoboken, NJ, USA: Wiley, 2009.

[19] J. Li and P. Stoica, "MIMO radar with colocated antennas," *IEEE Signal Process. Mag.*, vol. 24, no. 5, pp. 106–114, Sep. 2007.

[20] S. Boyd and L. Vandenberghe, *Convex Optimization*. Cambridge, U.K.: Cambridge Univ. Press, 2004.

[21] K. Gerlach and M. Steiner, "Fast converging adaptive processor or a structured covariance matrix," *IEEE Trans. Aerosp. Electron. Syst.*, vol. 36, no. 4, pp. 1115–1126, Oct. 2000.

[22] Y. I. Abramovich and O. Besson, "Regularized covariance matrix estimation in complex elliptically symmetric distributions using the expected likelihood approach—Part 1: The over-sampled case," *IEEE Trans. Signal Process.*, vol. 61, no. 23, pp. 5807–5818, Dec. 2013.

[23] A. De Maio, L. Pallotta, J. Li, and P. Stoica, "Loading factor estimation under affine constraints on the covariance eigenvalues with application to radar target detection," *IEEE Trans. Aerosp. Electron. Syst.*, vol. 55, no. 3, pp. 1269–1283, Jun. 2019.

[24] G. Cui, H. Li, and M. Rangaswamy, "MIMO radar waveform design with constant modulus and similarity constraints," *IEEE Trans. Signal Process.*, vol. 62, no. 2, pp. 343–353, Jan. 2014.

[25] O. Aldayel, V. Monga, and M. Rangaswamy, "Successive QCQP refinement for MIMO radar waveform design under practical constraints," *IEEE Trans. Signal Process.*, vol. 64, no. 14, pp. 3760–3774, Jul. 2016.

[26] Z. Cheng, Z. He, B. Liao, and M. Fang, "MIMO radar waveform design with PAPR and similarity constraints," *IEEE Trans. Signal Process.*, vol. 66, no. 4, pp. 968–981, Feb. 2018.

[27] A. De Maio, Y. Huang, M. Piezzo, S. Zhang, and A. Farina, "Design of optimized radar codes with a peak to average power ratio constraint," *IEEE Trans. Signal Process.*, vol. 59, no. 6, pp. 2683–2697, Jun. 2011.

[28] Z.-Q. Luo, W.-K. Ma, A. So, Y. Ye, and S. Zhang, "Semidefinite relaxation of quadratic optimization problems," *IEEE Signal Process. Mag.*, vol. 27, no. 3, pp. 20–34, May 2010.

[29] M. Grant, S. Boyd, and Y. Ye. (2009). *CVX: MATLAB Software for Disciplined Convex Programming*. [Online]. Available: <http://www.stanford.edu/~boyd/cvxbook>



**YIQIN CHEN** received the B.Sc. degree from the School of Mechanical and Electronic Information, China University of Geosciences, in 2003, the M.Sc. degree from the School of Computer and Electronic Information, Guangxi University, in 2007, and the Ph.D. degree from the School of Optical and Electronic Information, Huazhong University of Science and Technology, in 2015. He is currently holds a postdoctoral position with the School of Electronic and Optical Engineering, Nanjing University of Science and Technology, Nanjing, China.



**MATTHEW RITCHIE** (Senior Member, IEEE) received the M.Sc. degree in physics from Nottingham University, in 2008, and the Ph.D. degree in engineering from University College London (UCL), in 2013, association with Thales, U.K. He is currently a Lecturer within the UCL Sensors, Systems and Circuits Group, UCL, with Prof. H. Griffiths focusing on passive radar, multistatic radar, FMCW radar micro-Doppler, and machine learning. His research interests include human micro-Doppler analysis, including gait and gesture recognition, micro-drones detection, tracking and classification, passive bistatic radar for air traffic control, and sea clutter analysis.



**WEIMIN SU** received the Ph.D. degree from the Nanjing University of Science and Technology, Nanjing, China, in 1998. He is currently a Professor with the Nanjing University of Science and Technology, a Senior Member of the Chinese Institute of Electronics, and a member of the Signal Processing Society of China. His research interests include signal processing technology and advanced SAR systems.



**YUJIU ZHAO** received the B.Eng. degree in electronic information engineering from the Nanjing University of Science and Technology, Nanjing, China, in 2013, where he is currently pursuing the Ph.D. degree. Since 2018, he has been a Visiting Student with the Department of Electrical and Electronic Engineering, School of Communications and Signal Processing, Imperial College London, London, U.K. Since 2019, he has been a Visiting Student with the Sensors, Systems and

Circuits Group, Department of Electrical and Electronic Engineering, University College London, London, U.K. His research interest includes MIMO radar signal processing, especially on MIMO radar waveform designing and optimization theory.



**HONG GU** received the M.S. degree from the Nanjing University of Science and Technology, Nanjing, China, in 1991, and the Ph.D. degree from Xidian University, China, in 1995. He is currently a Professor with the Nanjing University of Science and Technology, a Senior Member of the Chinese Institute of Electronics, and a member of the Radar Branch of the Jiangsu Electronic Society. His research interests include noise SAR, radar signal processing, and information systems.

• • •